EXPERIMENTAL STUDY OF THE SPONTANEOUS IGNITION OF PARTLY CONFINED HYDROGEN JETS

Maxwell, B.M.[1], Tawagi, P.[1] and Radulescu, M.I.[1]
[1] Department of Mechanical Engineering, University of Ottawa, 161 Louis Pasteur, Ottawa, K1N 6N5, Canada, bmaxw005@uottawa.ca

ABSTRACT

The current study addresses the spontaneous ignition of hydrogen jets released into a confined oxidizer environment, experimentally. The experiments are conducted in a shock tube where hydrogen gas is shock-accelerated into oxygen across a perforated plate. The operating conditions and hole dimension of the plate were varied in order to identify different flow field and ignition scenarios. Time resolved Schlieren visualization permitted to reconstruct the gasdynamic evolution of the release and different shock interactions. Time resolved self-luminosity records permitted us to record whether ignition was achieved, and also to record the dimension of the turbulent mixing layer. The ignition limits determined experimentally in good agreement with the 1D diffusion ignition model proposed by Maxwell and Radulescu. Nevertheless, the experiments demonstrated that the mixing layer is two to three orders of magnitude thicker than predicted by molecular diffusion, which can be attributed to the observed mixing layer instabilities and shock-mixing layer interactions, which provide a much more intense mixing rate than anticipated from previous and current numerical predictions. These observations further clarify why releases through partly confined geometries are more conducive to jet ignition of the jets.

1.0 INTRODUCTION

When pressurized hydrogen is suddenly released into air, experiments[1-6] have reproducibly demonstrated that spontaneous ignition of the release is possible. Numerous ignition mechanisms have been postulated, see the recent review by Astbury and Hawksworth[7]. Among these different mechanisms, the diffusion-ignition mechanism is currently believed to be the dominating one. In this mechanism, the rapidly expanding hydrogen jet drives a shock wave that heats the air. Since chemical reactions require both fuel and oxidizer to be present simultaneously, localized ignition spots may occur within the diffusion layer where both the cold fuel and the shock heated air co-exist. Detailed numerical simulations of both confined and unconfined releases[8-16] have identified this mechanism as being responsible for localized combustion, giving rise to local “hot spots”.

The experiments[2-6] have only been able to determine spontaneous ignition limits, for hydrogen releases, providing the hydrogen jet is first released through a partly confining tube. Furthermore, ignition of unconfined releases was not observed when partly confined jets did ignite. Since these observations, the influence of the tube confinement has been of active investigation[3-6,12-15]. Also, since detailed diagnostics are not available experimentally within the relatively narrow extension tubes used, most experiments could not monitor the fast flow field development within the extension tubes and nor explain the promoting effect that a tube has on ignition. Typical holes and extension tubes considered in these experiments are on the order of the centimetre. Instead, most studies used Computational Fluid Dynamics (CFD) tools to investigate the propensity for ignition in confined environments. Based on these simulations, different mechanisms have been proposed. Maxwell and Radulescu[8] have suggested that confinement of the releases prevents the jet from gasdynamic expansion. The volumetric expansion cooling was shown by Maxwell and Radulescu to be the dominating mechanism preventing ignition[8]. Likewise, Bragin and Molkov[16] have proposed that local heating in the boundary layers also promotes ignition. Likewise, shock reflections from the confinement walls, and further shock focusing at the jet axis, was found to provide local temperature

increases conducive to ignition. In reality, it is likely that all these mechanisms control the local temperature in the mixing layer and its propensity for ignition.

One fundamental aspect, however, that has not been adequately addressed by previous studies is the influence of mixing in the confined jets. It is believed that ignition of the jet not only depends on temperature in the diffusion layer alone, but also on the amount of turbulent mixing between the fuel and the oxidizer. Dryer et al.[2] suggested that confined releases may exhibit more mixing through the Richtmyer-Meshkov instability[17,18] that is promoted when transverse shocks interact with the mixing layer, akin to the mixing of unreacted pockets in gaseous detonations by transverse shock waves[19]. They postulate that larger volumes of premixed or reacted gases exiting the tube permits the establishment of a self-sustained jet flame at the exit. Bragin and Molkov[16] further substained this mechanism, which relies on the entrainment of burned gases into the re-circulating vortices in jets. It is thus not unreasonable to expect that ignition of the jet is controlled not only by the condition that local hotspots are created in the tube[8], but also more importantly by *how much* gases have ignited inside the tube. The amount of ignited gas depends intimately on turbulent mixing and local temperature variations through shock reflections[6]. In this sense, a confining extension is likely to provide both an increase in mixing and high temperatures to promote ignition.

Unfortunately, CFD investigations generally cannot adequately treat compressible turbulent mixing, due to the very small scales required to adequately solve compressible turbulent reactive flows. Likewise, the lack of experimental data on the jet evolution within the confinement are also lacking due to the difficulty of experimentally monitoring the rapidly evolving flow fields on such small scales.

The current study addresses this fundamental ignition process in partly confined releases *experimentally*. To address the small scale limitations of previous experiments of H_2 jet releases in confining tubes, we decided to *scale up* the experiment and consider larger hole releases (hole sizes which range from 2-7 centimetres) through a 20 cm confinement. Although clearly not realistic of hydrogen releases, the scaling up of these experiments permits us to implement several visualisation diagnostics and pressure measurements in order to monitor with adequate space and time resolution the evolution of the hydrodynamic flow field obtained when hydrogen is released into an oxidizer through a hole in partly confined spaces. The results of the detailed experiments, other than elucidating the physical processes leading to jet ignition with regards to hydrogen explosion safety considerations, may also be very useful in future benchmarking of numerical strategies.

The paper is organized as follows. Section 2 presents the details of the experimental technique developed in our laboratory to study the ignition of hydrogen jets in confined geometries. Section 3 provides the experimental results for the flow field evolution and ignition events. Section 4 provides numerical simulations of the flow field, which complement our experimental results. Section 5 compares the ignition limits obtained experimentally with the one-dimensional numerical model recently formulated by Maxwell and Radulescu[8]. Since the model neglects any wave reflection, it permits to further gauge the importance of these effects on the hot-spot and jet ignition criteria.

2.0 EXPERIMENTAL METHOD

In order to study the spontaneous ignition of hydrogen jets in partially confined environments, we used a shock tube technique illustrated in Figure 1. The shock tube is 3m long and has a rectangular cross section area of 203mm high by 19mm wide. The narrowness of its cross section in one direction permits us to establish flow fields that are essentially two-dimensional. The experimental setup, inspired by Wolanski and Wojcicki's experiment[1], consists of a test section where hydrogen gas is initially separated from oxygen by a diaphragm and a 12mm thick perforated plate with a single rectangular hole. The two hole sizes under investigation in this study are $d=20$mm and $d=67$mm

openings; both of which are 19mm wide. An acetylene-oxygen driver is used to drive a strong shock wave through the test section, causing hydrogen to flow into oxygen.

Prior to conducting the experiment, each chamber is evacuated below 50 Pa before it is filled with the respective gas. The test sections are then filled with pure oxygen and hydrogen to 3.5±0.1 kPa and 3.4±0.1 kPa, respectively. The oxygen section is pressurized slightly more than the hydrogen to ensure that the diaphragm rests against the hole in the constrictor plate. The driver section contains stoichiometric acetylene-oxygen mixture, whose initial pressure is varied and controls the jet strength. A detonation is first initiated in the driver section by a spark plug located at the end wall as shown in Figure 1. Once the resulting detonation wave reaches the first diaphragm, a shock wave transmits into the hydrogen, whose strength is controlled by the initial pressure of the driver. When the incident shock wave breaks the second diaphragm, the compressed hydrogen expands into the oxygen section, driving a strong shock wave ahead of the jet.

To capture any resulting combustion, a high speed PIV camera (PCO.2000) is used to take direct time resolved self-luminosity photo records of the jet with an exposure time of 4μs. The viewing area of the camera is illustrated in Figure 1, with its left edge located 25.4mm downstream from the hole. In separate experiments, the camera is used to capture pairs of time resolved Schlieren photographs, an imaging technique which uses refraction of light in a fluid to capture density gradients[20]. The Schlieren system uses 12 inch field mirrors and a stroboscopic light source delivering two successive sub-microsecond time flashes with inter-flash time of a few microseconds. This permitted us to perform Schlieren velocimetry of the various shock speeds and density gradients in the flow field with microsecond time resolution. Finally, the shock tube is equipped with 4 pressure sensors, as shown in Figure 1. Sensors S1 and S2 are used to estimate the strength of the incident shock which travels through the hydrogen and also to estimate the time at which the hydrogen jet begins to burst into the oxygen section. Sensors S3 and S4 are used to acquire the trigger timings for the camera.

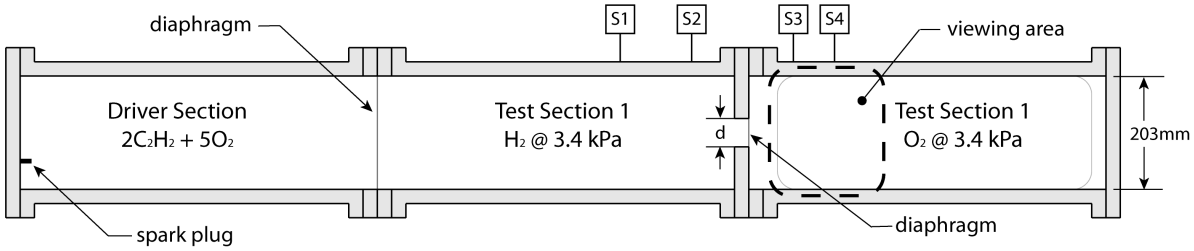

Figure 1. Shock tube setup for hydrogen release experiment. Each section of the shock tube is separated by diaphragms, shown, and filled with the respective gas. The cross section of the shock tube is 203mm high by 19mm wide. The two hole sizes under investigation in this study are *d=20*mm and *d=67*mm.

3.0 EXPERIMENTAL RESULTS

3.1 Evolution of an Expanding Jet Into a Partially Confined Space

A series of Schlieren photographs were taken for jets of similar conditions, at different times, in order to construct a flow field of how the jet evolves upon its release into the confined environment. The frames shown below in Figure 2 all correspond to cases where the driver pressure was kept constant at 12.4±0.1 kPa, and the test sections for oxygen and hydrogen were also kept constant at 3.5±0.1 kPa and 3.4±0.1 kPa, respectively. The hole size used to reconstruct the flow field was the 67mm hole. In the early stages of release, Figure 2*a*, the expanding jet drives a shock wave into the oxygen, which is curved due to expansion into the larger cross sectional area of the shock tube. At approximately 300 μs into the release process, the leading shock wave reflects from the top and bottom walls, as can be seen in Figure 2*b* and 2*c*. Due to the large amounts of turbulence associated with the hydrogen jet, it is

difficult to see how the reflected shock wave transmits into the jet, a feature that is investigated below in numerical simulations. Despite this, however, the reflected shock wave can be seen travelling in the transverse direction within the shocked oxygen in the subsequent frames of Figure 2. Finally, shortly after the shock reflection at the wall, a secondary shock wave is observed travelling in the axial direction of the jet. This secondary shock wave was found to travel from the jet surface towards the leading shock wave, as can be seen in Figures 2*c*, 2*d*, and 2*e*. Eventually, this shock wave catches up with the leading shock wave as can be seen in Figure 2*f*. It should be noted that the actual location of the release hole is 25.4mm to the left of each photo in Figure 2. The origin of this secondary shock wave, determined in numerical simulations below, is the shock reflection process from the confinement walls.

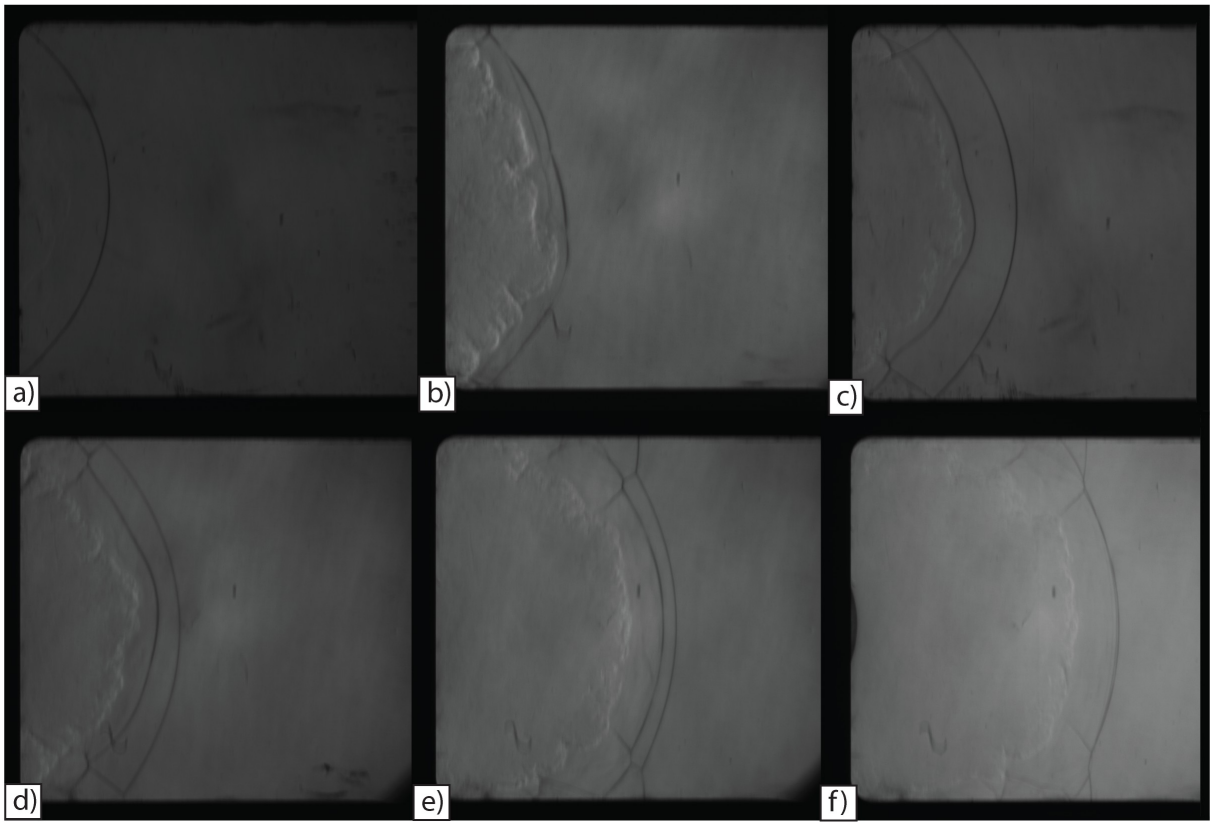

Figure 2. Evolution of a hydrogen jet release into a confined oxidizer environment. These Schlieren photographs were captured for the 67mm hole size at various times; a) 262μs b) 312μs, c) 318μs, d) 346μs, e) 382μs, and f) 407μs after the jets initial release into oxygen..

3.2 Ignition Results

A series of experiments have been conducted for the two different hole sizes, in order to find their corresponding ignition limits. In the experiments, the pressure of the driver gas was varied to drive different strength shocks into the test sections. The pressures of the test sections, hydrogen and oxygen, were kept constant. A summary of the various experiments, including their parameters and principle observations, is shown in Table 1. Also shown in the table are the estimated strengths of the incident and transmitted shocks, in the hydrogen and oxygen sections, respectively.

In Figure 3a, a Schlieren image is shown for an expanding hydrogen jet into oxygen for a case where ignition was detected for the 67mm opening (experiment 1 from Table 1). The particular image in this figure was taken approximately 290μs into the release process. Typical images showing the combustion of jets under similar conditions, experiments 2 and 3, are shown in Figures 3b and c,

respectively. These two figures were taken approximately 310μs and 400μs after the jet was released into oxygen. Of particular interest in Figure 3b are the two evident hotspots on the top and bottom walls of the shock tube. The increased luminosity in these regions suggests that the combustion resulting from reflected shock waves interacting with the expanding jet is much more intense then elsewhere along the jet surface. It is believed that this locally intense combustion is a result of increased local mixing due the Richtmyer–Meshkov instability[17,18]. Finally, Figure 3c shows complete ignition of the entire jet at a later time. To confirm that the images in Figures 3b and c are showing combustion, the experiment is repeated by substituting the oxygen with nitrogen. In this case, experiment 4, no self-emission was recorded, thus confirming the observed combustion in the previous experiments.

Also, of particular interest is the size of the combustion zone. In Figures 3b and c, the entire jet has been ignited, and not just a thin region at the head of the jet. According to Maxwell and Radulescu[8], the size of the diffusion layer at the head of the jet is in the order of approximately 1-100 μm. In the experiments, however, the combustion zone spans several centimetres. Also in Figure 3b, there is a zone of combustion along the axis of the jet, located near the hole which is located far away from the surface of the jet; this was found to be due to enhanced turbulent mixing, see below the results of the numerical experiments.

Table 1. Experimental Results.

Test #	Driver pressure (kPa)	Estimated driver gas detonation Mach #	Incident shock in H_2 (Mach #)	Transmitted shock in O_2 (Mach #)	Observation
67mm opening					
1	14.8	6.7	3.4	5.6	Full jet ignition detected
2	14.8	6.7	3.5	5.8	Full jet ignition detected
3	14.8	6.7	3.4	5.6	Full jet ignition detected
4	14.8	6.7	3.4	5.6	H_2 into N_2 (no ignition)
5	13.8	6.7	3.7	6.2	Full jet ignition detected
6	12.4	6.6	3.3	5.4	Full jet ignition detected
7	12.4	6.6	3.1	5	Full jet ignition detected
8	14.8	6.7	2.9	4.6	Full jet ignition detected
9	11.7	6.6	2.9	4.6	No ignition detected
10	12.1	6.6	2.7	4.2	No ignition detected
11	8.8	6.6	2.3	3.4	Hotspot found on top wall
12	10.3	6.6	2.5	3.8	No ignition detected
13	10.3	6.6	2.6	4	No ignition detected
14	10.3	6.6	2.5	3.8	Hotspot found on top wall
20mm opening					
15	16.2	6.7	3.6	6	Full jet ignition detected
16	16.5	6.7	3.5	5.8	Full jet ignition detected
17	14.8	6.7	3.4	5.6	Full jet ignition detected
18	14.1	6.7	3.3	5.4	Full jet ignition detected
19	15.5	6.7	3.2	5.2	Full jet ignition detected
20	13.8	6.7	3.1	5	Full jet ignition detected
21	13.4	6.6	3.1	5	Full jet ignition detected
22	13.1	6.6	3.2	5.2	No ignition detected
23	13	6.6	3	4.8	No ignition detected
24	13.1	6.6	3	4.8	No ignition detected
25	14.5	6.7	2.9	4.6	No ignition detected
26	14.8	6.7	2.9	4.6	No ignition detected
27	13.8	6.7	2.8	4.4	Full jet ignition detected

In the remainder of the experiments for the *d=67*mm case, the pressure of the driver was varied in order to find the conditions for which the jet did not ignite upon release into oxygen. The ignition limit for this particular hole size (67mm) was found to be around a transmitted shock strength into oxygen of *M=4.6±0.4*. Interestingly, a third regime was observed, in experiments 11 and 14, where local ignition hot spots appear near the top wall of the shock tube but do not lead to complete ignition of the jet. These hotspots are shown in Figures 4*a* and 3*b*, respectively. Furthermore, upon repeating the experiment with the *d=20*mm hole size, the ignition limit was found to be around a transmitted shock strength into oxygen of *M=5.1±0.3*, which was slightly higher than that of the 67mm hole.

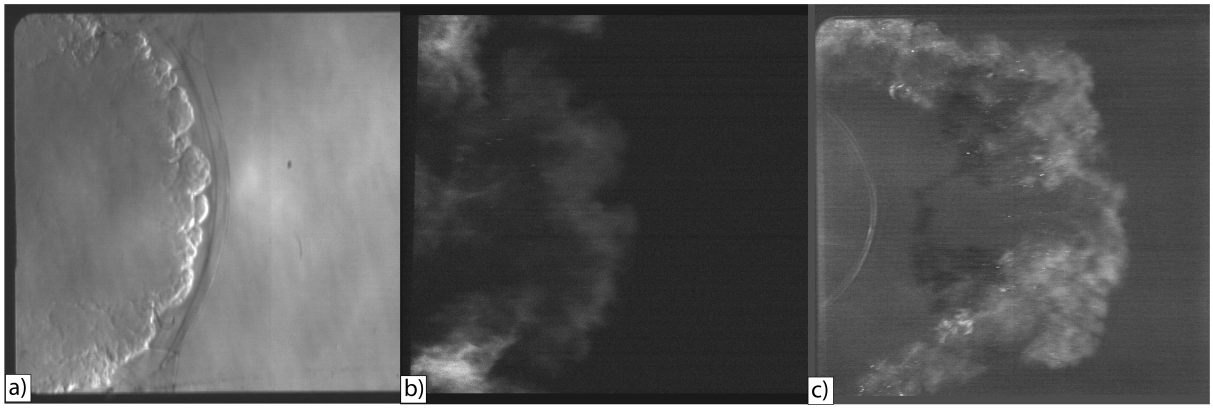

Figure 3. Typical cases where full jet ignition is observed. Frame a) is a Schlieren image showing density gradients of the expanding hydrogen jet into oxygen at approximately 290μs into the release process. Frames b) and c) show the combustion occurring at approximately 310μs and 400μs into the release process, respectively.

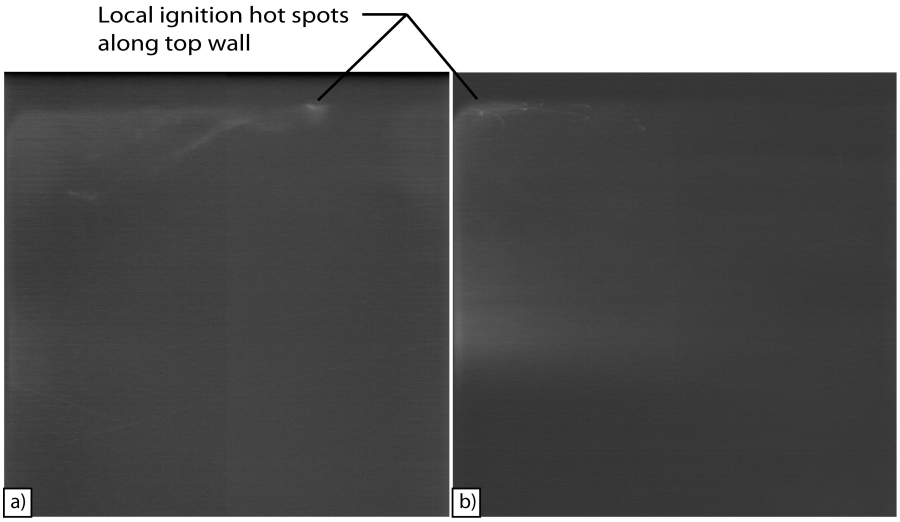

Figure 4. Images showing localized ignition hot spots for cases where complete jet ignition does not occur, corresponding to experiments 11 (a) and 14 (b), respectively.

4.0 NUMERICAL RECONSTRUCTION OF THE FLOW FIELD

To further aid in the interpretations of the experimental results presented above, we have also reconstructed the evolution of the flow field using detailed numerical simulations of the confined releases. The present calculations focus on the gasdynamic evolution of the flow field and turbulent advection. They do not address ignition nor molecular mixing, which would require very fine

resolutions not currently accessible through direct numerical simulations. We thus solved numerically the two-dimensional non-reactive inviscid Euler equations, shown below in equations 2-6, where perfect gas behaviour is assumed.

$$\frac{\partial \rho}{\partial t}+\nabla\cdot(\rho u)=0\,, \tag{2}$$

$$\frac{\partial \rho u}{\partial t}+\nabla\cdot(u(\rho u))+\nabla p=0\,, \tag{3}$$

$$\frac{\partial \rho E}{\partial t}+\nabla\cdot(u(E+p))=0\,, \tag{4}$$

where

$$E=\rho e+\frac{1}{2}\rho u^2\,, \tag{5}$$

$$\frac{p}{\rho}=RT\,, \tag{6}$$

To solve these governing equations, Godunov's[21] exact Riemann solver was used. The AMRITA software system[22] is used for the numerical implementation. The domain for the simulation is the experimental setup illustrated in Figure 1 with the 67mm hole size. The resolution used in the simulation was 256 grid points across the hole. An adaptive mesh refinement technique permitted us to afford the required resolution to monitor the detailed flow evolution and hydrodynamic instabilities.

The initial conditions for the pressure, density, and velocity are shown below in Figure 5. The test sections are representative of the stagnant hydrogen and oxygen states used in the experiment from Section 2.1 at 3.4 kPa. To initiate the experiment, and to drive a shock wave into the test section, the Taylor expansion wave profile[23] is applied in the driver section as can be seen in Figure 5. The Taylor expansion wave profile is the post-detonation profile of pressure, density, and velocity once the detonation has reached the first diaphragm.

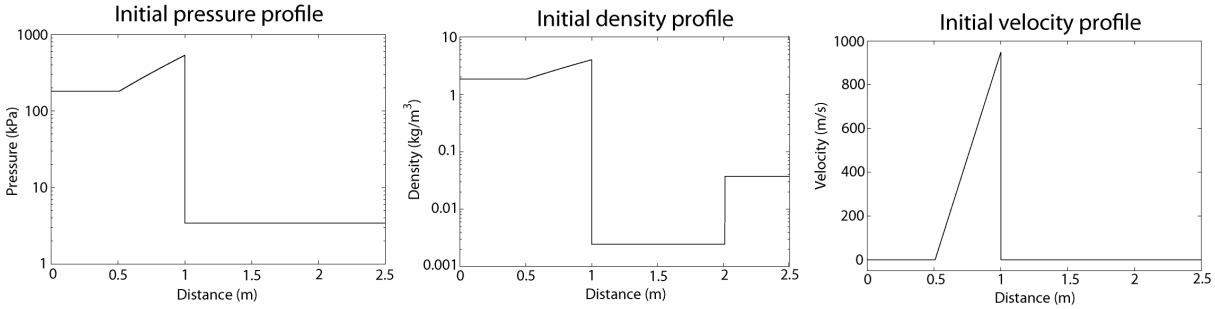

Figure 5. Initial profiles of pressure, density, and velocity for the non-reactive simulation.

Figure 6 shows the flow field evolution once the shock driven by the reactive driver has reached the perforated plate separating hydrogen and oxygen. The figure shows successive records of the density gradients. In Figure 6a, the incident shock wave driven by the expanding driver gas products is shown travelling towards the contact surface, which separates the stagnant hydrogen from the stagnant oxygen. In Figure 6b, the incident shock wave reflects from both the contact surface and the constrictor plate wall. Also, a leading shock wave is transmitted into the oxygen, which is driven by

the expanding pressurized hydrogen jet. In Figure 6*d*, the leading shock wave reflects from the top wall of the shock tube. A portion of the reflected shock wave is found to be transmitted into the hydrogen jet near the shock tube wall. Once the reflected shock wave transmits into the expanding hydrogen jet, it propagates at much higher speeds. This is due to the significantly high sound speed of hydrogen compared to oxygen.

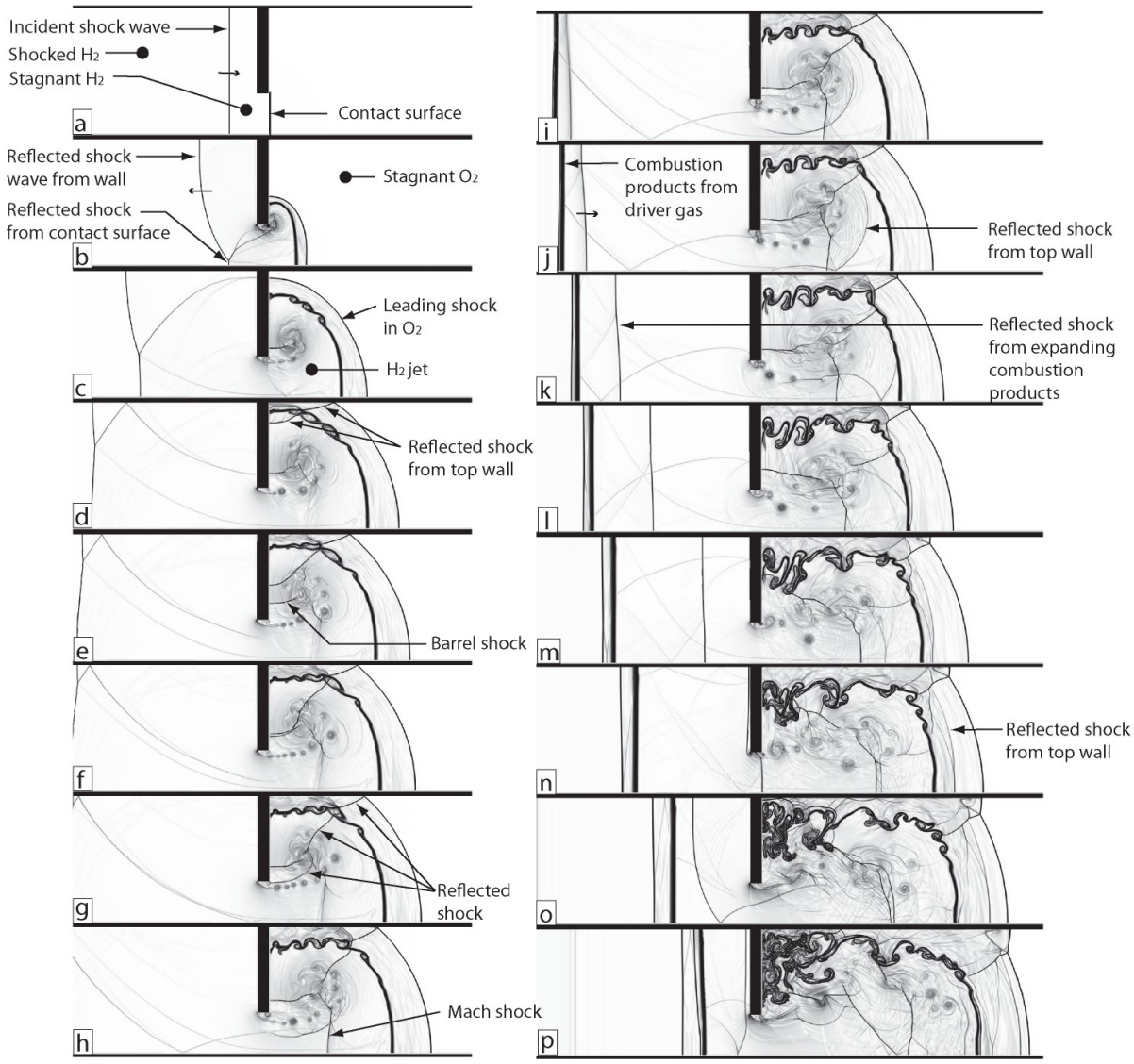

Figure 6. Non-reactive numerical simulation of hydrogen jet release experiment. The images above shows density gradients of the hydrogen jet evolution.

The numerical simulations of Figure 6 also shed significant insight into the experimental photographs of Figure 3 in regards to the very thick mixing layers observed experimentally. First, as can be seen from fames *f-m* of Figure 6, the sides of the mixing layer form shear layers: the hydrogen escaping across the corner acquires vortical motion, which shocked oxygen does not. This gives rise to Kelvin-Helmholtz instability on the mixing layer and increased mixing. This mixing layer further disrupted by the passage of the reflected shock from the wall, which is seen traversing the mixing layer in frame *e* of Figure 6. This interaction of the reflected shock wave with the jet causes the instabilities at the surface of the jet to grow at increased rates via the Richtmyer-Meshkov instability[17,18]. This leads to increased turbulence, which is clearly seen at the jet interface near the shock tube walls in the

subsequent frames of Figure 6. Also, this increased turbulence has the effect of increasing mixing rates and also causes the shocked oxygen to become entrained into the hydrogen jet. In Figures 6*f*, *g*, and *h*, the reflected shock wave propagates through the Barrel shock and Mach shock[24] and in Figure 6*i,* the reflected shock wave is found to be propagating towards the front of the jet. This shock wave, now travelling in the axial direction of the jet, is able to emerge into the shocked oxygen, well before the portion of the reflected shock wave travelling through the oxygen in the transverse direction is able to reach the jet axis, as can be seen in Figure 6*l*. The effect of this shock wave on the surface of the jet is to further promote increased turbulent mixing on the front of the jet, again through the Richtmyer-Meshkov instability. In the subsequent frames of Figure 6, it can be seen that this reflected, or secondary shock wave eventually catches up with the lead shock wave, as observed in the experiments, and also in previous numerical simulations[15].

Finally, in Figure 7 and 8, the vorticity and corresponding density is shown at two times of the release process. At an early time, prior to the jets interaction with the reflected shock wave, it is clear from Figure 7 that the shear layer between the jet and shocked oxygen becomes unstable due to Kelvin-Helmholtz instability. A number of small vortices appear on the shear layer which act to entrain the shocked oxygen into the jet. Also shown in Figure 7 is a large vortex that appears near the hole. In Figure 8, which corresponds to a much later time, well after the jet has been disturbed by the reflected shock wave, it is clear that the entire jet has become completely unstable and turbulent due to both the Kelvin-Helmholtz and Richtmyer-Meshkov instabilities. These instabilities, coupled with the central vortex near the hole, all contribute to enhanced mixing and entrainment of the shocked oxygen into the jet. Furthermore, in the experiments, the jet is even more turbulent than the numerical simulations, suggesting that even more pockets of oxygen and burned products are entrained into the jet. This explains the large combustion zones observed experimentally along the jet surface, and also the combustion zone located within the middle of the jet near the hole.

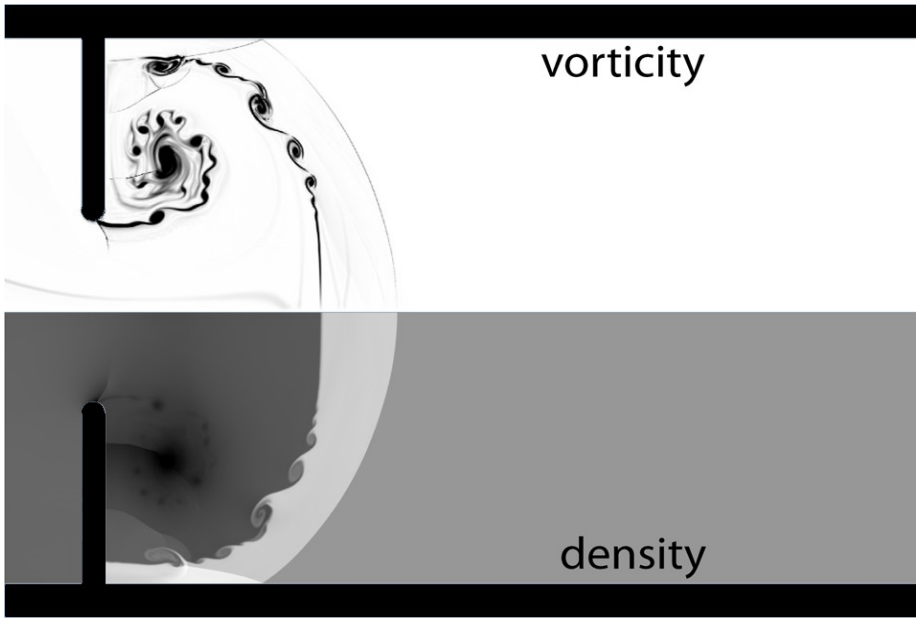

Figure 7. Vorticity (top) and density (bottom) plots for an instance of the jet evolution at an early time, prior to the jet interaction with the reflected shock wave.

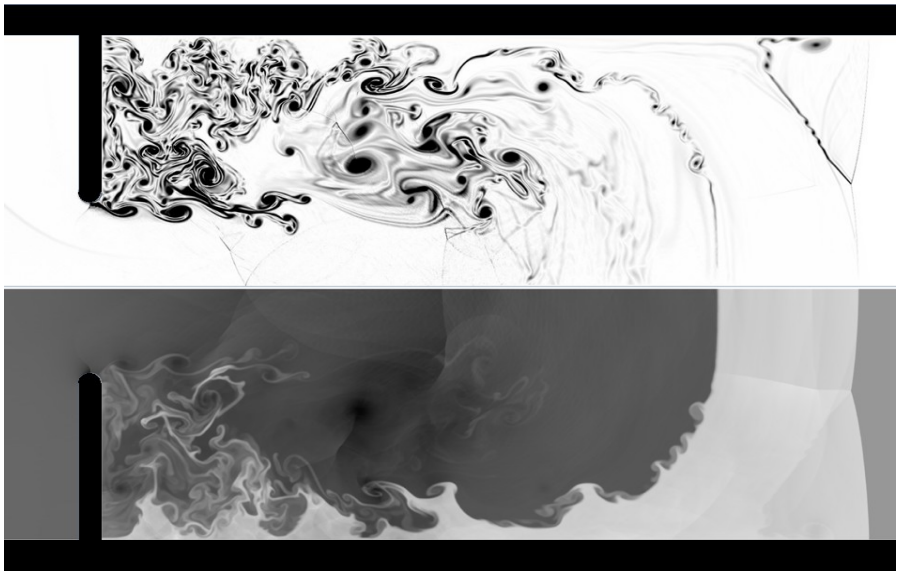

Figure 8. Vorticity (top) and density (bottom) plots for an instance of the jet evolution at a much later time when the entire jet becomes unstable and turbulent.

5.0 INITIAL SHOCK HEATING OF THE INTERFACE AND IGNITION LIMITS

In order to quantify the conditions for when ignition occurred during a release, we first determined the state of the contact surface immediately after the incident shock breaks out across the perforated plate. At the perforated plate, this problem is a one-dimensional gasdynamic problem, solved by determining the wave interactions at the hole. These are illustrated in Figure 9. Since the incident shock is transmitted into a medium with a higher acoustic impedance (ρc), there will be a reflected shock wave, as can be seen from the numerical simulations of Figure 6. The state of the interface after the interaction and Mach numbers of the transmitted shock can be simply obtained by matching the pressures and particle speed at the interface. Given the strength of the incident shock, as measured by the pressure sensors 1 and 2, the state of the interface and the transmitted shock are readily determined. Table 1 lists this information.

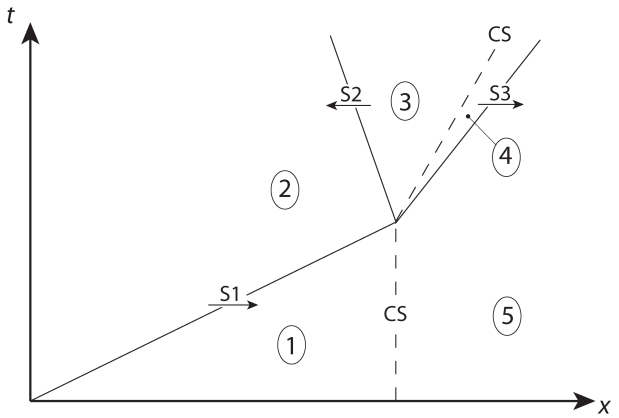

Figure 9. An *x-t* diagram illustrating the interaction of a shock wave (S1) propagating through the undisturbed hydrogen (zone 1) with a contact surface (cs) separating undisturbed oxygen (zone 5) from the hydrogen. Also shown in the figure are the reflected shock wave (S2), the transmitted shock wave (S3). Also labelled are the shocked states of hydrogen (zone 2 and 3) and also the shocked state of oxygen (zone 4).

With the knowledge of the initial shock heating of the diffusion layer, we can estimate the potential of the mixing layer to ignite using the model formulated by Maxwell and Radulescu[8]. The model takes into account the rapid expansion of the mixing layer as a quenching mechanism, but not any further shock reflections, nor any subsequent turbulent mixing. It thus only provides the prediction if the gases ignite, but not how much of the gas ignites.

The model is a localized one-dimensional description of the thin diffusion layer at the head of the jet, in Lagrangian coordinates. Realistic thermodynamic properties, reaction rates, and transport properties are taken into account. The rate at which the pressure decays in the diffusion layer is prescribed as a source term. Specific details of the model are found in [8]. To adapt the model to the experiment described in this paper, known information about states 3 and 4 from Figure 8 are applied as the initial conditions of the diffusion layer. Also, the pressure decay rate source term is adapted to the two dimensional slit jet geometry of this experiment.

The ignition limits predicted for the two hole sizes are given below in Table 2. They are given in terms of the transmitted shock strength into oxygen. Table 2 also provides the ignition limit observed experimentally. Close agreement is observed between the numerical model and the experiments. The experimental limits are found to be slightly less than the numerical limits.

The main difference between the model predictions and the experiment is the amount of gas that has reacted. Owing to molecular diffusion, a one-dimensional diffusion layer, at the time of observation of Figure 3, is expected to be less than 1 millimetre thick. Instead, the mixing layer that has undergone ignition in the experiments was found to be 1 to 2 orders of magnitude thicker. This discrepancy can be due to the effects of diaphragm rupture, which are known to provide increased disturbances in the flow, but also to Kelvin-Helmholtz and Richtmyer-Meshkov instabilities in the flow, as captured in the simulations above. Clearly, more experiments are required at early times to monitor the effect of the diaphragm rupture, However, these non-idealities are not without interest, as real releases of hydrogen will also be subjected to the same effects.

Table 2. Ignition Limits Comparison.

Hole size (mm)	Experimental ignition limit (Mach #)*	Numerical ignition limit – 1D model[7] (Mach #)*
67	4.6±0.4	4.7±0.1
20	5.1±0.3	5.5±0.1

* shock strength given for the transmitted shock in O_2

6.0 CONCLUSION

In this study, shock induced diffusion ignition of pressurized hydrogen jets flowing into a confined oxidizer environment has been studied experimentally using a novel approach. Results of the experiments reveal that the ignition limits of hydrogen releases into confined environments depends strongly on the strength of the shock wave that is driven into oxygen ahead of the jet, and also size of the hole through which hydrogen escapes. Numerical simulations in this study reveal that Kelvin-Helmholtz and Richtmyer-Meshkov instabilities lead to increased turbulent mixing rates and thus cause large amounts of oxygen to become entrained into the jet. For this reason, much more gas is ignited than predicted by previous numerical investigations[12,15].

Finally, the experiments were compared with the ignition limits predicted by a one-dimensional model[8]. It was found that unconfined releases have only a slightly higher ignition limit then the partially confined releases in the experiments. Despite this slight deviation, the model is able to predict the ignition limit with fairly close agreement, suggesting that the reflected shock waves only provide further ignition of the jet. In cases when the lead shock does not ignite the gas, reflected

shocks only ignite isolated spots near the walls. The reflected shock waves, however, play a major role in influencing turbulent mixing within the jet, and thus how the ignition spots interact to ignite the entire jet.

This work was sponsored by the NSERC Hydrogen Canada (H2CAN) Strategic Research Network and by an NSERC Discovery Grant. B.M.M. also acknowledges financial support by the Ontario Ministry of Training, Colleges and Universities via an Ontario Graduate Scholarship.

1. Wolanski P. and Wojcicki S. (1973). 14th Symp. (Int.) on Combustion, Pittsburg, PA 1217-1223.
2. Dryer F. L., Chaos M., Zhao Z., Stein J. N., Alpert J. Y., and Homer C. J. (2007). Combust. Sci. Tech. 179: 663-694.
3. Golovastov S. V., Baklanov D. I., Volodin V. V., Golub V. V., and Ivanov K. V. (2009). Russ. J. Phys. Chem. B 3 No. 3: 348-355.
4. Mogi T., Wada Y., Ogata Y., and Hayashi A. K. (2009). Int. J. Hydrogen Energy 34: 5810-5816.
5. Oleszczak P. and Wolanski P. (2010). Shock Waves 20:539-550.
6. Lee H.J., Kim Y.R., Kim S.H., and Jeung I.S. (2011). Proceedings of the Combustion Institute 33: 2351-2358.
7. Astbury G.R., and Hawksworth S.J. (2007). Int. J. Hydrogen Energy 32: 2178-2185.
8. Maxwell B. M., and Radulescu M.I. (2011). Combust. Flame doi: 10.1016/j.combustflame.2011.03.001 (In press)
9. Liu Y. F., Tsuboi F. N., Sato H., Higashino F, and Hayashi A. K. (2005). 20th Intl Colloquium on the Dynamics of Explosions and Reactive Systems, Montreal, Canada.
10. Liu Y. L., Zheng J. Y., Xu P., Zhao Y. Z., Bei H. Y., Chen H. G., and Dryver H. (2009). Journal of Loss Prevention in the Process Industries 22: 265-270.
11. Xu B. P., Hima L. E. L., Wen J. X., and Tam V. H. Y. (2009). Int. J. Hydrogen Energy 34 No. 14: 5954-5960.
12. Wen J. X., Xu B. P., and Tam V. H. Y. (2009). Combust. Flame 156: 2173-2189.
13. Xu B. P., Hima L. E., Wen J. X., Dembele S., Tam V. H. Y., and Donchev T. (2008). Journal of Loss Prevention in the Process Industries 21: 205-213.
14. Yamada E., Kitabayashi N., Hayashi A. K., and Tsuboi N. (2011). Int. J. Hydrogen Energy 36: 2560-2566.
15. Lee B.J., and Jeung I. (2009). Int. J. Hydrogen Energy 34: 8763-8769.
16. Bragin M.V., and Molkov V.V. (2011). Int. J. Hydrogen Energy 36: 2589-2596.
17. Ricthmyer R.D. (1960). Commun. Pure Appl. Math 13: 297-313.
18. Meshkov Y. Y. (1969). Soviet Fluid Dynamics 4: 101-104.
19. Radulescu M.I., Sharpe G.J., Law C.K., and Lee J.H.S. (2007). J. Fluid Mech. 580: 31-81.
20. Settles G. S. (2001). Schlieren and Shadowgraph Techniques, Springer-Verlag
21. Godunov S. K. (1959). Math. Sbornik 47: 271-306.
22. Quirk J.J. (1998). 29th Computational Fluid Dynamics, von Karman Institute Lecture Series.
23. Taylor G.I. (1950) Proc. R. Soc. Lond. A 201 No. 1065: 159-174.
24. Radulescu M. I., and Law C. K. (2007). J. Fluid Mech. 578: 331-369.
25. Liepmann H. W. and Rhoshko A. (2001). Elements of Gas Dynamics, Dover.